https://doi.org/10.1016/j.apenergy.2019.114060

A cost-effective and chemically stable electrode binder for alkaline-acid direct ethylene glycol fuel cells

Zhefei Pan, Yanding Bi, Liang An*

Department of Mechanical Engineering, The Hong Kong Polytechnic University, Hung Hom, Kowloon, Hong Kong SAR, China.

*Corresponding author.

Email: liang.an@polyu.edu.hk (L. An)

Abstract

In preparing direct liquid fuel cell electrodes, an ionomer is necessary, whose functions are not only to bind the discrete catalyst nanoparticles onto the substrate materials to build the porous catalyst layer, but also to construct the triple phase boundaries to provide continuous pathways for reactant delivery. In this work, a cost-effective and chemically stable poly(vinylidene fluoride-co-hexafluoropropylene) electrode binder is adopted and compared with the conventional Nafion and polytetrafluoroethylene in terms of the electrode morphology and the fuel cell performance. It is found that the fuel cell using the poly(vinylidene fluoride-co-hexafluoropropylene)-based electrode exhibits the best performance in terms of an open-circuit voltage of 1.47 V, a maximum current density of 300 mA cm^{-2}, and a peak power density of 120.0 mW cm^{-2}. Comparing to the fuel cell performances fabricated with the conventional Nafion and polytetrafluoroethylene as electrode binder, the peak power density achieved by using the new type of electrode binder shows an improvement of 13.7% and 58.1%, respectively. Poly(vinylidene fluoride-co-hexafluoropropylene) shows the lowest cost of \$0.18 kW^{-1}, while polytetrafluoroethylene and Nafion possess the higher cost of \$0.80 kW^{-1} and \$145.59 kW^{-1}, respectively. The impressive improvement is attributed to the fact that the poly(vinylidene fluoride-co-

hexafluoropropylene)-based electrode has a higher electrochemical surface area due to its intrinsic porous property, enhancing the anodic reaction kinetics. It is found that the best cell performance is achieved with 1.0 M EG and 5.0 M KOH in the anolyte and 1.0 M H_2O_2 and 4.0 M H_2SO_4 in the catholyte at 60°C

Keywords: Direct ethylene glycol fuel cells; Electrode binder; Hydrogen peroxide; Operating parameters; Power density

1. Introduction

As two global issues of climate change and energy crisis are becoming severer, proton exchange membrane fuel cells (PEMFCs) that use hydrogen as fuel and oxygen/air as oxidant have received ever-increasing attention as an alternative energy production technology in the last several decades [1, 2], which is primarily due to their intrinsic superiorities such as high efficiency [3, 4], simple design [5, 6], low emissions [7, 8], and quick refueling [9, 10]. Apart from the great achievements made in PEMFCs that use proton exchange membranes (PEMs) as ion exchange membranes (IEMs) [11, 12], anion exchange membrane fuel cells (AEMFCs) using anion exchange membranes (AEMs) as IEMs have attracted worldwide research interest, which is mainly ascribed to the fact that non-precious metal nanocatalysts can be used in AEMFCs due to the enhanced reaction kinetics rendered from the alkaline environment, thus the cost of the fuel cell is significantly reduced [13, 14]. However, the production, storage, and transport of hydrogen are still the critical issues in the commercialization of hydrogen fuel cells, which need to be addressed [15]. Recently, direct liquid fuel cells (DLFCs) using liquid alcohols and soluble organics instead of gaseous hydrogen as the fuel have obtained tremendous development, which is regarded as one of the most promising power sources for portable electronics [16, 17]. In addition to the above-mentioned advantages, the DLFCs possesses a broader range of advantages including mature production, easy transportation, and convenient handling of liquid fuels comparing to gaseous hydrogen [18, 19]. Among the widely used alcohols such as methanol, ethanol, and ethylene glycol (EG), EG has received considerable interests because of the electron transfer rate as high as 80%, the boiling point of 198ºC, and the theoretical energy capacity of 4.8 Ah mL^{-1}, which is a promising fuel for portable electronic devices [20, 21]. Hence, direct ethylene glycol fuel cells (DEGFCs) become one of the research hotspots in DLFCs [22]. An et al. [23] developed and tested an alkaline DEGFC using an AEM, which yielded a peak power density

of 67 mW cm^{-2} at 60ºC. The excellent performance was attributed to the alkaline environment, which much promotes the kinetics of both the oxygen reduction reaction (ORR) and ethylene glycol oxidation reaction (EGOR). Considering the poor stability of the AEM at high temperatures, generally over 60ºC, they replaced the AEM with an alkali-doped polybenzimidazole in an alkaline DEGFC, which allows the operation of the fuel cell at higher temperatures (90ºC). As a result, it was found that a higher peak power density of 112 mW cm^{-2} was achieved at 90ºC [24]. To further promote the cell performance, Pan et al. [25] reported that an open-circuit voltage (OCV) of 1.41 V and a peak power density of 80.9 mW cm^{-2} at 60ºC were achieved by replacing the oxygen with hydrogen peroxide in an alkaline DEGFC. This type of DEGFC boosted the OCV by 62.1% and the peak power density by 20.8%, as well as eliminated the requirement of the air from the ambient environment. To improve the specific energy density and volumetric energy density, as well as extend the application situations to underwater and outer space, they developed a passive DEGFC with hydrogen peroxide as oxidant. This fuel cell exhibited peak power densities of 30.3 and 65.8 mW cm^{-2} at 23 and 60ºC, respectively [26]. They further developed and tested a passive DEGFC stack, which yielded an OCV of 3.0 V, a maximum current of 860 mA, and a peak power of 1178 mW at room temperature [27]. The passive stack was applied to power an electric fan for around 3 hours under the mimetic underwater circumstance, indicating that this passive stack can be air-independent power sources for underwater and outer space applications.

Similar to hydrogen fuel cells, in the preparation of the DLFC electrodes, an ionomer is necessary and plays an important role in the electrode fabrication. The ionomer possesses two functions. One is to bind the discrete catalyst nanoparticles onto the substrate materials to build the porous catalyst layer (CL), and the other is to construct the triple phase boundaries (TPBs) providing pathways for ion transport [28]. Generally, Nafion and

polytetrafluoroethylene (PTFE) are two ionomers that have been widely used in fuel cells [29]. Although Nafion has proved to be a promising ionomer in forming the CL, the cost is the main concern hindering its wide applications [30]. The price of the 5 wt. % Nafion dispersion is as high as \$4 mL^{-1} [31]. Choudhury et al. [32] prepared polyvinyl alcohol chemical hydrogel (PCH) and chitosan chemical hydrogel (CCH) as electrode binder for direct borohydride fuel cells (DBFCs) a chemical cross-linking reaction. Because of the hydrophilic property and thus high water-retention capability, the CCH performed better than the Nafion binder, and the PCH showed similar performance comparing to the Nafion binder. An et al. [29] synthesized agar chemical hydrogel (ACH) as electrode binder in a fuel-electrolyte-fed fuel cell. It yielded a peak power density of 380 mW cm^{-2} at 90^{o}C. PTFE is a cheaper binder comparing to Nafion. The price of the 60 wt. % PTFE dispersion is \$0.312 mL^{-1} [33]. However, one disadvantage of using PTFE as the electrode binder is that the reactants are not able to penetrate the PTFE binder [29]. For this reason, once the active sites in the catalyst layer, which are essential for electrochemical reactions, are covered by PTFE, the covered part would be not accessible and cannot catalyze the electrochemical reactions, resulting in the decrease in the electrochemical surface area (ECSA) [29].

Poly(vinylidene fluoride-co-hexafluoropropylene) (PVDF-HFP), an emerging fluorocopolymer, has been solely used or composited with other polymers to act as the membrane electrolyte in Li-ion batteries [34, 35]. Because of the copolymerization effect, PVDF–HFP has relatively low crystallinity. Hence, it contains more amorphous domains capable of trapping a large amount of liquid electrolytes [34]. For this reason, its superiority comparing to PTFE is that even though the active sites in the catalyst layer may be covered by PVDF-HFP, they are still capable to catalyze the electrochemical reactions, leading to a higher ECSA. In addition, the price of PVDF-HFP powder is \$0.12 g^{-1} [36], which is much cheaper than Nafion. Therefore, the cost of the fuel cell can be substantially reduced when

used in the electrode fabrication. In this work, three electrodes with different binders including PTFE, Nafion, and PVDF-HFP are prepared and then assembled into a DEGFC using acidified hydrogen peroxide as oxidant. It is found that the peak power densities achieved by PTFE, Nafion, and PVDF-HFP are 75.9, 105.5, and 120.0 mW cm^{-2} at 60°C, respectively. Impressively, the fuel cell performance achieved by using the PVDF-HFP-based electrode as anode is even higher than that using the Nafion-based one. In addition, PVDF-HFP shows the lowest cost of \$0.18 kW^{-1}, while PTFE and Nafion possess the higher cost of \$0.80 kW^{-1} and \$145.59 kW^{-1}, respectively. Considering the practical applications of DLFCs in portable electronics, electric vehicles, and stationary stations, PVDF-HFP can be the candidate to replace expensive Nafion functioning as the electrode binder, which meets the crucial requirement of low cost for worldwide commercialization.

2. Working principle

As shown in Fig. 1, the fuel cell is constituted by an anode, a CEM between the anode and the cathode, a cathode CL, and a cathode DL, forming the membrane electrode assembly (MEA), as well as two flow fields providing the anolyte and the catholyte. The anolyte flows in the flow channel, which is usually driven by a peristaltic pump, and the reactants transport from the flow field through the anode DL to the anode CL. Then, the EGOR takes place in the anode CL, where EG is oxidized to produce electrons, oxalate and water in the presence of hydroxide ions as shown below [22]:

$$C_2H_6O_2+10OH^-\rightarrow(COO^-)_2+8e^-+8H_2O \qquad E_{EGOR}=-0.69\ V \qquad (1)$$

The produced electrons are transferred from the anode to cathode through the external circuit driven by the potential difference between the anode and cathode. In the cathode, the hydrogen peroxide combining the existing protons and arrived electrons is reduced to water in the hydrogen peroxide reduction reaction (HPRR) according to the equation [37]:

$$4H_2O_2+8H^++8e^-\rightarrow8H_2O \qquad E_{HPRR}=1.78\ V \qquad (2)$$

Meanwhile, the current loop is completed by forming an internal ionic circuit via the potassium ions transferring through the CEM from the anode to cathode, driven by an electric field. Therefore, the overall reaction of this fuel cell is obtained by combining the EGOR and HPRR, which is shown as follows:

$$C_2H_6O_2+4H_2O_2+8H^++10OH^-\rightarrow(COO^-)_2+16H_2O \qquad E=2.47\ V \qquad (3)$$

It is impressive that the theoretical voltage of this fuel cell is as high as 2.47 V, which is much higher than that of the DLFCs using oxygen as oxidant, such as direct methanol fuel cells (1.21 V) [38], direct ethanol fuel cells (1.14 V) [39], and direct formate fuel cells (1.45 V) [40].

3. Experiment

3.1. Preparation of the membrane electrode assembly

Three membrane electrode assemblies (MEAs) were prepared in this work with different binder materials on the anodes, including Nafion, PTFE and PVDF-HFP. The MEAs consist of three components: an anode, a cathode and a CEM with a thickness of 30 μm (Nafion 211). Both electrodes were in-house fabricated with the same active area of 1.0 cm × 1.0 cm. To prepare the Pd/C anodes, dip-coating method was applied, which has been reported in previous publication [41]. When Nafion was used as the binder, the catalyst ink was prepared by mixing 30 wt. % Pd/C (Sigma-Aldrich Co., USA) with 5 wt.% Nafion (Fuel Cell Store, USA) and ethanol, which serves as the binder and solvent, respectively. Then, the catalyst ink was stirred in an ultrasonic bath for 20 minutes to disperse it uniformly. Subsequently, the nickel foam (Hohsen Co., Japan) with designed shape was dipped in the catalyst ink for 1 min before withdrawing it from the ink. Afterwards, the nickel foam was dried in the air by a blower. These two steps were repeated continuously until reaching the required catalyst coating, which is 1.0 mg_{Pd} cm^{-2} for the anode. The preparation of the anode with 60 wt. % PTFE (Fuel Cell Store, USA) and PVDF-HFP (Solvay S. A., France) as binders adopted the

same method except that acetone was used as the solvent for PVDF-HFP. The Au/C cathode was prepared by the spray method, which has been reported previously [42]. Firstly, 60 wt. % Au/C (Permetek Co., USA) was mixed with 15 wt. % Nafion and ethanol for the preparation of the catalyst ink. Subsequently, it was placed in an ultrasonic bath for 20 minutes. Lastly, the ink was sprayed onto the carbon cloth (Hesen, China), until a catalyst loading of 2.66 mg_{Au} cm^{-2} on the cathode was achieved. The CEMs used in the MEAs were obtained by the following treatments [42]: (1) cut the original Nafion 211 membranes to the designed shape of 1.5 cm × 1.5 cm, (2) immerse the membranes into an aqueous solution of 2.5 M KOH, (3) heat up the solution to 80ºC for 1 h, and (4) use DI water to rinse the membranes for several times and store them in DI water before the fuel cell assembly.

3.2. Cyclic voltammetry

Cyclic voltammetry (CV) tests were conducted in a three-electrode electrochemical cell, where the fabricated electrode, the Pt foil, and the Hg-HgO (MMO, 1.0 M KOH) were used as the working electrode, the counter electrode and the reference electrode, respectively. The CV curves were recorded by an electrochemical workstation (PGSTAT302N). The potential window for the CV tests was from −1.126 to 0.074 V at a scan rate of 50 mV s^{-1}.

3.3. Fuel cell setup and instrumentation

The whole fuel cell was assembled by fixing the MEA in between an anode plate and a cathode plate. The material of the plates is 316L stainless steel to avoid the corrosion problem caused by the anolyte and catholyte. In addition, flow fields were grooved on both plates with a single serpentine shape. The flow fields have a width of 1.0 mm and a depth of 0.5 mm. The electrolytes on anode and cathode were fed into the flow fields by utilizing two peristaltic pumps with a flow rate of 2 mL min^{-1}. The electrochemical impendence spectra (EIS) test was conducted with a CHI 605C (CH Instruments, China). Moreover, to examine the effects of the operating temperatures on the cell performance, two electrical heating rods

were used to heat up the cell, and the temperature was measured and controlled by a thermocouple and a temperature controller, respectively. To evaluate the fuel cell performance, an Arbin BT2000 (Arbin Instrument Inc.) was utilized to measure the polarization curves.

4. Results and discussion

4.1. General performance

Fig. 2 shows the general performance of the fuel cell fed with anolyte containing 1.0 M EG and 1.0 M KOH and catholyte containing 1.0 M H_2O_2 and 1.0 M H_2SO_4, both of which are at a flow rate of 2 mL min^{-1}, running with three home-made electrodes using different binders at room temperature with pretreated Nafion 211 membrane as the CEM. It is seen that the fuel cell using PVDF-HFP as the electrode binder showed the highest voltage over the whole current density region, followed by the Nafion binder, and the fuel cell using the PTFE binder output the worst cell voltage. The OCVs of PVDF-HFP and Nafion were similar at around 1.18 V, while the OCV of PTFE was a little lower at around 1.14 V. In addition, the peak power densities achieved by the PVDF-HFP, Nafion, and PTFE were 31.9, 27.5, and 20.8 mW cm^{-2}, respectively. Therefore, among three electrode binders, PVDF-HFP is the best choice to be applied in alkaline-acid DEGFCs as an electrode binder, which is not only due to the highest power output, but also the lowest price as compared previously.

4.2. Characterization of three as-prepared electrodes

To find the reasons why PVDF-HFP performs better than Nafion and PTFE, CV tests and scanning electron microscope (SEM) characterizations are implemented for the fabricated electrodes and SEM tests are conducted for the binders at dry state as well. Fig. 3 shows the CV curves of three electrodes in 1.0 M KOH solution at a scan rate of 50 mV s^{-1}. It can be seen that the electrode with PVDF-HFP as the binder possessed the highest peak area of the reduction of PdO ranging from -0.8 to -0.2 V, indicating that the electrode with PVDF-HFP

yielded the largest ECSA. The ECSA can be calculated by the PdO reduction charge in the CV curves as shown in Equation (4):

$$\mathrm{ECSA}= \frac{Q}{qm} \tag{4}$$

where Q is the coulombic charge, q is the charge value of 405 μC cm^{-2} for the reduction of PdO monolayer, and m is the Pd loading on the electrode [43, 44]. Based on the equation, the ECSAs of the three electrodes with PVDF-HFP, Nafion, and PTFE are 24.10, 18.62, and 16.44 m^2 g^{-1}, respectively. Hence, the remarkable performance of PVDF-HFP is attributed to the higher ECSA, which provides more active sites for the EGOR. Figs. 4 (a), (b) and (c) show the SEM images of the PVDF-HFP, Nafion, and PTFE at dry state, respectively. It is found that the PVDF-HFP tends to form a porous structure with small particles accumulation together. In contrast, the Nafion tends to form a film structure with a smooth surface. The roughness of the PTFE is in between the PVDF-HFP and Nafion. Therefore, it can be inferred from the structures that Nafion tends to be clad on the catalyst nanoparticles when used as the binder in the electrode fabrication, thus the ECSA is decreased significantly. When PVDF-HFP is employed as the binder, it tends to adhere the catalyst nanoparticles onto the nickel foam skeleton but not to cover the catalyst nanoparticles, so that the PVDF-HFP-based electrode has the highest ECSA [28]. Although the PTFE-based electrode is supposed to have the higher ECSA than the Nafion-based electrode according to the morphology of the binders at dry state, the Nafion-based electrode actually possesses the higher ECSA. This abnormal phenomenon can be explained as follows. As Nafion is permeable to reactants [29], the active sites covered by Nafion are still accessible to the reactants, indicating that the total active sites of the Nafion-based electrode having the catalytic ability include not only the uncovered active sites but also a number of active sites covered by the binder. In addition, the reactants are not able to penetrate the PTFE binder, so the total active sites of the PTFE-based electrode are merely the uncovered active sites. As a result, the additional active sites of the

Nafion-based electrode compensate the disparity between the Nafion-based electrode and the PTFE-based electrode, leading to the higher ECSA of the Nafion-based electrode.

Fig. 5 shows Nyquist plots of the present fuel cell using three different electrodes at room temperature. The ohmic resistance and charge transfer resistance dominate in the high-frequency region, while the mass transport resistance dominates in the low‑frequency region [45]. It is found that the arcs of the impedance spectra in high‑frequency region are similar, suggesting that the charge transfer resistances of fuel cells using these three electrodes are near. It also can be seen from the intersections of the curves and horizontal axis that the PVDF-HFP-based electrode possesses the lowest ohmic resistance, followed by the Nafion-based electrode, and the PTFE-based electrode results in the largest ohmic resistance. This observation also accounts for the fuel cell performance variations. Due to the lowest ohmic resistance, the PVDF-HFP-based electrode yields the best fuel cell performance. The lowest ohmic resistance may be attributed to the partial covered catalyst particles, thus the exposed catalyst particles contribute to the higher conductivity.

4.3. Fuel cell performance

Fig. 6 shows the polarization and power density curves of fuel cells with three different electrodes at the previously optimized reactant-feeding concentrations, *i.e.* 1.0 M EG and 5.0 M KOH in the anolyte and 4.0 M H_2O_2 and 1.0 M H_2SO_4 in the catholyte, at room temperature. Comparing to the cell performance fed with 1.0 M EG and 1.0 M KOH in the anolyte and 1.0 M H_2O_2 and 1.0 M H_2SO_4 in the catholyte, the cell performance with three binders all shows great improvements in OCVs, maximum current densities, and peak power densities. It is seen that the OCV of the cell using PTFE binder increases from 1.14 V to 1.31 V and the OCVs of the cells with PVDF-HFP and Nafion increase from 1.18 V to 1.39 V and 1.18 V to 1.38 V, respectively. In addition, the increases in maximum current densities of the PVDF-HFP, Nafion, and PTFE are 25, 10, and 30 mA cm^{-2}, respectively. Due to the

elevations in both the cell voltage and current densities, the peak power densities boost significantly from 31.9 to 57.0 mW cm^{-2} with PVDF-HFP binder, from 27.4 to 46.1 mW cm^{-2} with Nafion binder, and from 20.8 to 39.9 mW cm^{-2} with PTFE binder. This performance improvement can be explained as follows. For the specific anode and cathode, the concentrations of reactants in the CLs have the dominant effect on the reaction kinetics. As the reactant-feeding concentrations are low, the reactant concentrations in the CLs are at starvation state, thus the reaction kinetics is sluggish. When the reactant concentrations increase, the delivery of the reactants from the flow field through the DL to the CL is enhanced, which is derived from the higher concentration gradient. As a result, the reactant concentrations in the CLs transfer from the starvation state to the saturation state, hence the reaction kinetics is enhanced.

Fig. 7 shows the polarization and power density curves of fuel cells with three different electrodes fed with 1.0 M EG and 1.0 M KOH in the anolyte and 1.0 M H_2O_2 and 1.0 M H_2SO_4 in the catholyte at 60ºC. It is found that the cell performance with three binders all has conspicuous enhancement in OCVs, maximum current densities, as well as peak power densities. It is seen that the OCV of the cell using PTFE binder increases from 1.14 V to 1.23 V and the OCVs of the cells with PVDF-HFP and Nafion increase from 1.18 V to 1.24 V and 1.18 V to 1.22 V, respectively. Meanwhile, the increases in maximum current densities of the PVDF-HFP, Nafion, and PTFE are 25, 15, and 25 mA cm^{-2}, respectively. In addition, the peak power densities increase dramatically from 31.9 to 56.3 mW cm^{-2} with PVDF-HFP binder, from 27.4 to 42.1 mW cm^{-2} with Nafion binder, and from 20.8 to 28.5 mW cm^{-2} with PTFE binder. The impressive improvement in the fuel cell performance is attributed to the elevated operating temperature, which can be illustrated by three reasons Firstly, increasing the operating temperature enhances the reaction kinetics of the EGOR in the anode and the HPRR in the cathode simultaneously, which lowers the activation loss. Secondly, the

mobility of electrons and diffusivity of reactants are promoted with at higher operating temperatures, leading to the fact that the reactants can reach the active sites on the CLs more efficiently, thus the concentration loss is reduced. Lastly, as the operating temperature increases, the viscosity of the anolyte and catholyte decreases and the conductivity of CEMs increases, which reduces the ohmic loss. Therefore, the fuel cell yields a better performance at higher operating temperatures due to the decreases in activation loss, concentration loss, and ohmic loss.

Fig. 8 shows the polarization and power density curves of fuel cells with three different electrodes at the reactant-feeding concentrations of 1.0 M EG and 5.0 M KOH in the anolyte and 1.0 M H_2O_2 and 4.0 M H_2SO_4 in the catholyte at 60ºC. It is found that the best cell performance in OCVs, maximum current densities, and peak power densities is achieved combining the increased reactant-feeding concentrations and higher operating temperature. It is shown that the OCVs of the cell using PVDF-HFP, Nafion, and PTFE are 1.47 V, 1.46 V, and 1.45 V, respectively. Meanwhile, the maximum current densities of the PVDF-HFP, Nafion, and PTFE show great improvements, which are 300, 220, and 195 mA cm^{-2}, respectively. In addition, comparing to the fuel cell performance fed with 1.0 M EG and 1.0 M KOH in the anolyte and 1.0 M H_2O_2 and 1.0 M H_2SO_4 in the catholyte at room temperature, the peak power densities increase dramatically from 31.9 to 120.0 mW cm^{-2} with PVDF-HFP binder, from 27.4 to 105.5 mW cm^{-2} with Nafion binder, and from 20.8 to 75.9 mW cm^{-2} with PTFE binder. The tremendous enhancement in power densities is attributed to the positive effects brought by increasing reactant-feeding concentrations and operating temperature. The maximum peak power density of 120.0 mW cm^{-2} is 48.3% higher than that achieved in our previous publication (80.9 mW cm^{-2}) [25]. The only difference is the fabrication method of the electrode, which is dip-coating method rather than the brushing method, suggesting that the dip-coating method is superior than the brushing method when

nickel foam is used as the backing layer. The reasons can be summarized as follows. For the same catalyst loading, the CL formed on the surface of nickel foam by the brushing method is much thicker and denser, which may result in large agglomerates lowering the catalyst utilization efficiency. Conversely, the CL formed on the skeleton of nickel foam by the dip-coating method is much thinner and sparser, which improves the catalyst utilization efficiency, thus the ECSA of the electrode using the dip-coating method is higher than that using the brushing method [41]. Moreover, the dense CL formed by the brushing method has the low porosity and small pore size, resulting in a low permeability and high transport resistance, while the electrode using the dip-coating method has the higher porosity and larger open pores, thus the permeability is higher. Hence, mass transport is enhanced through the porous electrode using the dip-coating method, reducing the fuel cell resistance [44].

4.4. Transient discharging behavior

Fig. 9 demonstrates the transient discharging behavior of the fuel cell using the PVDF-HFP-based and Nafion-based electrodes fed with 1.0 M EG and 5.0 M KOH in the anolyte and 1.0 M H_2O_2 and 4.0 M H_2SO_4 in the catholyte at 60°C. It is indicated that the fuel cell using PVDF-HFP-based electrode exhibits a stable output voltage around 0.8 V with acceptable fluctuations for 100 h at a discharging current density of 100 mA cm^{-2}. The voltage fluctuation may be attributed to the decomposition of H_2O_2 and thus generation of O_2, forming a two-phase flow in the cathode flow channel. It creates a large transport resistance of H_2O_2 from the cathode flow channel to the cathode CL [46]. The stable running time of the fuel cell is twenty times as long as the fuel cell using the sprayed electrode (5 h) [25], which is attributed to the dip-coated electrode having the higher porosity and larger open pores, thus the efficient reactant-feeding and product-removing are achieved, contributing to stabilizing the cell voltage. The outstanding stability indicates that this DEGFC with the PVDF-HFP-based electrode fabricated using the dip-coating method possesses the potential for future

practical applications. Although the voltage of Nafion electrode is higher than the PVDF-HFP-based electrode at the initial 20 h, the Nafion-based electrode experiences an obvious voltage degradation at the rest 80h, while the PVDF-HFP-based electrode shows a rather stable voltage at the same discharging current density. It implies that PVDF-HFP-based electrode has a longer life-time in this fuel cell.

4.5. Cost estimation

Table 1 shows the cost estimation and comparison of three electrode binders in the fuel cell and the cost is evaluated according to the equation (5):

$$C = \frac{1000 \times 1000 \times UP \times m}{PP} \quad (5)$$

where C is the cost of the electrode binder in the fuel cell normalized by power output, UP is the unite price of the binder, m is the mass of the used binder, and PP is the peak power generated by the fuel cell with the electrode binder obtained previously. It is seen that PVDF-HFP shows the lowest cost of \$0.18 kW^{-1}, while PTFE and Nafion possess the higher cost of \$0.80 kW^{-1} and \$145.59 kW^{-1}, respectively. The significant reduction in cost is attributed the lower unit price of PVDF-HFP and the higher peak power achieved by the fuel cell using PVDF-HFP as the electrode binder.

5. Concluding remarks

In this work, the cost-effective poly(vinylidene fluoride-co-hexafluoropropylene) is used to replace the conventional and expensive Nafion and polytetrafluoroethylene as the binder in the electrode fabrication. The home-made electrodes using these binders are characterized via cyclic voltammetry and scanning electron microscope. In addition, they are assembled into an alkaline-acid direct ethylene glycol fuel cell and evaluated in terms of the fuel cell performance. The results show that the ECSAs of the electrodes with PVDF-HFP, Nafion, and PTFE are 24.10, 18.62, and 16.44 $m^2 g^{-1}$, respectively. It is because PVDF-HFP tends to adhere the catalyst nanoparticles onto the nickel foam skeleton but not to cover the catalyst

nanoparticles, thus the PVDF-HFP-based electrode has the highest ECSA. In performance tests, the fuel cell using the PVDF-HFP-based electrode exhibits the best performance of an open-circuit voltage of 1.47 V, a maximum current density of 300 mA cm^{-2}, and a peak power density of 120.0 mW cm^{-2} with 1.0 M EG and 5.0 M KOH in the anolyte and 4.0 M H_2O_2 and 1.0 M H_2SO_4 in the catholyte at 60°C. Comparing to the cell performance with conventional Nafion and polytetrafluoroethylene as the electrode binder, the peak power density shows an improvement of 13.7% and 58.1%, respectively. The impressive improvement is attributed to the higher ECSA due to its intrinsic porous property, contributing to the enhancement in the reaction kinetics. It is found that PVDF-HFP shows the lowest cost of \$0.18 kW^{-1}, while PTFE and Nafion possess the higher cost of \$0.80 kW^{-1} and \$145.59 kW^{-1}, respectively. The significant reduction in cost is attributed the lower unit price of PVDF-HFP and the higher peak power achieved by the fuel cell using PVDF-HFP as electrode binder.

Acknowledgement:

This work was fully supported by a grant from the Research Grants Council of the Hong Kong Special Administrative Region, China (Project No. 25211817).

References

[1] Pan ZF, An L, Zhao TS, Tang ZK. Advances and challenges in alkaline anion exchange membrane fuel cells. Progress in Energy and Combustion Science 2018;66:141-75.

[2] An L, Zhao T. Anion exchange membrane fuel cells: principles, materials and systems: Springer; 2018.

[3] Pan ZF, An L, Wen CY. Recent advances in fuel cells based propulsion systems for unmanned aerial vehicles. Applied Energy 2019;240:473-85.

[4] Sun X, Li Y. Understanding mass and charge transports to create anion-ionomer-free high-performance alkaline direct formate fuel cells. International Journal of Hydrogen Energy 2019;44:7538-43.

[5] Larminie J, Dicks A, McDonald MS. Fuel cell systems explained: J. Wiley Chichester, UK; 2003.

[6] Li Y, Feng Y, Sun X. Insight into interface behaviors to build phase-boundary-matched Na-ion direct liquid fuel cells. ACS Sustainable Chemistry & Engineering 2018;6:12827-34.

[7] Wu QX, Pan ZF, An L. Recent advances in alkali-doped polybenzimidazole membranes for fuel cell applications. Renewable and Sustainable Energy Reviews 2018;89:168-83.

[8] Sun X, Li Y, Li M-J. Highly Dispersed Palladium Nanoparticles on Carbon-Decorated Porous Nickel Electrode: An Effective Strategy to Boost Direct Ethanol Fuel Cell up to 202 mW cm–2. ACS Sustainable Chemistry & Engineering 2019;7:11186-93.

[9] Dekel DR. Review of cell performance in anion exchange membrane fuel cells. Journal of Power Sources 2018;375:158-69.

[10] Wu Q, Li H, Yuan W, Luo Z, Wang F, Sun H, Zhao X, Fu H. Performance evaluation of an air-breathing high-temperature proton exchange membrane fuel cell. Applied energy 2015;160:146-52.

[11] Mahato N, Banerjee A, Gupta A, Omar S, Balani K. Progress in material selection for solid oxide fuel cell technology: A review. Progress in Materials Science 2015;72:141-337.

[12] Zhao X, Yuan W, Wu Q, Sun H, Luo Z, Fu H. High-temperature passive direct methanol fuel cells operating with concentrated fuels. Journal of Power Sources 2015;273:517-21.

[13] Kulkarni A, Siahrostami S, Patel A, Nørskov JK. Understanding catalytic activity trends in the oxygen reduction reaction. Chemical reviews 2018;118:2302-12.

[14] Gewirth AA, Varnell JA, DiAscro AM. Nonprecious metal catalysts for oxygen reduction in heterogeneous aqueous systems. Chemical reviews 2018;118:2313-39.

[15] Turner JA. Sustainable hydrogen production. Science 2004;305:972-4.

[16] Demirci UB. Direct liquid-feed fuel cells: thermodynamic and environmental concerns. Journal of Power Sources 2007;169:239-46.

[17] Wu Q, Zhao T, Chen R, An L. A sandwich structured membrane for direct methanol fuel cells operating with neat methanol. Applied energy 2013;106:301-6.

[18] Pan ZF, Chen R, An L, Li YS. Alkaline anion exchange membrane fuel cells for cogeneration of electricity and valuable chemicals. Journal of Power Sources 2017;365:430-45.

[19] Jiang J, Li Y, Liang J, Yang W, Li X. Modeling of high-efficient direct methanol fuel cells with order-structured catalyst layer. Applied Energy 2019;252:113431.

[20] Yue H, Zhao Y, Ma X, Gong J. Ethylene glycol: properties, synthesis, and applications. Chemical Society Reviews 2012;41:4218-44.

[21] Pan Z, Bi Y, An L. Mathematical modeling of direct ethylene glycol fuel cells incorporating the effect of the competitive adsorption. Applied Thermal Engineering 2019;147:1115-24.

[22] An L, Chen R. Recent progress in alkaline direct ethylene glycol fuel cells for sustainable energy production. Journal of Power Sources 2016;329:484-501.

[23] An L, Zhao T, Shen S, Wu Q, Chen R. Performance of a direct ethylene glycol fuel cell with an anion-exchange membrane. international journal of hydrogen energy 2010;35:4329-35.

[24] An L, Zeng L, Zhao T. An alkaline direct ethylene glycol fuel cell with an alkali-doped polybenzimidazole membrane. international journal of hydrogen energy 2013;38:10602-6.

[25] Pan Z, Huang B, An L. Performance of a hybrid direct ethylene glycol fuel cell. International Journal of Energy Research 2019;43:2583-91.

[26] Pan Z, Bi Y, An L. Performance characteristics of a passive direct ethylene glycol fuel cell with hydrogen peroxide as oxidant. Applied Energy 2019;250:846-54.

[27] Pan Z, Zhuang H, Bi Y, An L. A direct ethylene glycol fuel cell stack as air-independent power sources for underwater and outer space applications. Journal of Power Sources 2019;437:226944.

[28] Li Y, Zhao T, Liang Z. Effect of polymer binders in anode catalyst layer on performance of alkaline direct ethanol fuel cells. Journal of Power Sources 2009;190:223-9.

[29] An L, Zhao T, Zeng L. Agar chemical hydrogel electrode binder for fuel-electrolyte-fed fuel cells. Applied energy 2013;109:67-71.

[30] Zhang F, Chen G, Hickner MA, Logan BE. Novel anti-flooding poly (dimethylsiloxane)(PDMS) catalyst binder for microbial fuel cell cathodes. Journal of Power Sources 2012;218:100-5.

[31] Fang LN. The Preparation and Electrochemical Properties of Perovskite La0.6Sr0.4CoO3-d for Catalytic Reduction of Oxygen. International Journal of Electrochemical Science 2017;12:218-29.

[32] Choudhury NA, Ma J, Sahai Y, Buchheit RG. High performance polymer chemical hydrogel-based electrode binder materials for direct borohydride fuel cells. Journal of Power Sources 2011;196:5817-22.

[33] Luo Y, Jin C, Wang ZJ, Wei MH, Yang CH, Yang RZ, Chen Y, Liu ML. A high-performance oxygen electrode for Li-O-2 batteries: Mo2C nanoparticles grown on carbon fibers. Journal of Materials Chemistry A 2017;5:5690-5.

[34] Pu W, He X, Wang L, Jiang C, Wan C. Preparation of PVDF–HFP microporous membrane for Li-ion batteries by phase inversion. Journal of membrane science 2006;272:11-4.

[35] Miao R, Liu B, Zhu Z, Liu Y, Li J, Wang X, Li Q. PVDF-HFP-based porous polymer electrolyte membranes for lithium-ion batteries. Journal of Power Sources 2008;184:420-6.

[36] Beyer H, Metzger M, Sicklinger J, Wu X, Schwenke KU, Gasteiger HA. Antimony Doped Tin Oxide-Synthesis, Characterization and Application as Cathode Material in Li-O-2 Cells: Implications on the Prospect of Carbon-Free Cathodes for Rechargeable Lithium-Air Batteries. Journal of the Electrochemical Society 2017;164:A1026-A36.

[37] An L, Zhao T, Chen R, Wu Q. A novel direct ethanol fuel cell with high power density. Journal of Power Sources 2011;196:6219-22.

[38] Munjewar SS, Thombre SB, Mallick RK. Approaches to overcome the barrier issues of passive direct methanol fuel cell–Review. Renewable and Sustainable Energy Reviews 2017;67:1087-104.

[39] Badwal S, Giddey S, Kulkarni A, Goel J, Basu S. Direct ethanol fuel cells for transport and stationary applications–A comprehensive review. Applied Energy 2015;145:80-103.

[40] An L, Chen R. Direct formate fuel cells: a review. Journal of power sources 2016;320:127-39.

[41] Li Y, Zhao T. A high-performance integrated electrode for anion-exchange membrane direct ethanol fuel cells. international journal of hydrogen energy 2011;36:7707-13.

[42] An L, Zhao T. Performance of an alkaline-acid direct ethanol fuel cell. international journal of hydrogen energy 2011;36:9994-9.

[43] Li Y, Lv J, He Y. A monolithic carbon foam-supported Pd-based catalyst towards ethanol electro-oxidation in alkaline media. Journal of The Electrochemical Society 2016;163:F424-F7.

[44] Li Y, He Y. An all-in-one electrode for high-performance liquid-feed micro polymer electrolyte membrane fuel cells. Journal of The Electrochemical Society 2016;163:F663-F7.

[45] Orazem ME, Tribollet B. Electrochemical impedance spectroscopy: John Wiley & Sons; 2017.

[46] Zhao TS, Xu C, Chen R, Yang WW. Mass transport phenomena in direct methanol fuel cells. Progress in Energy and Combustion Science 2009;35:275-92.

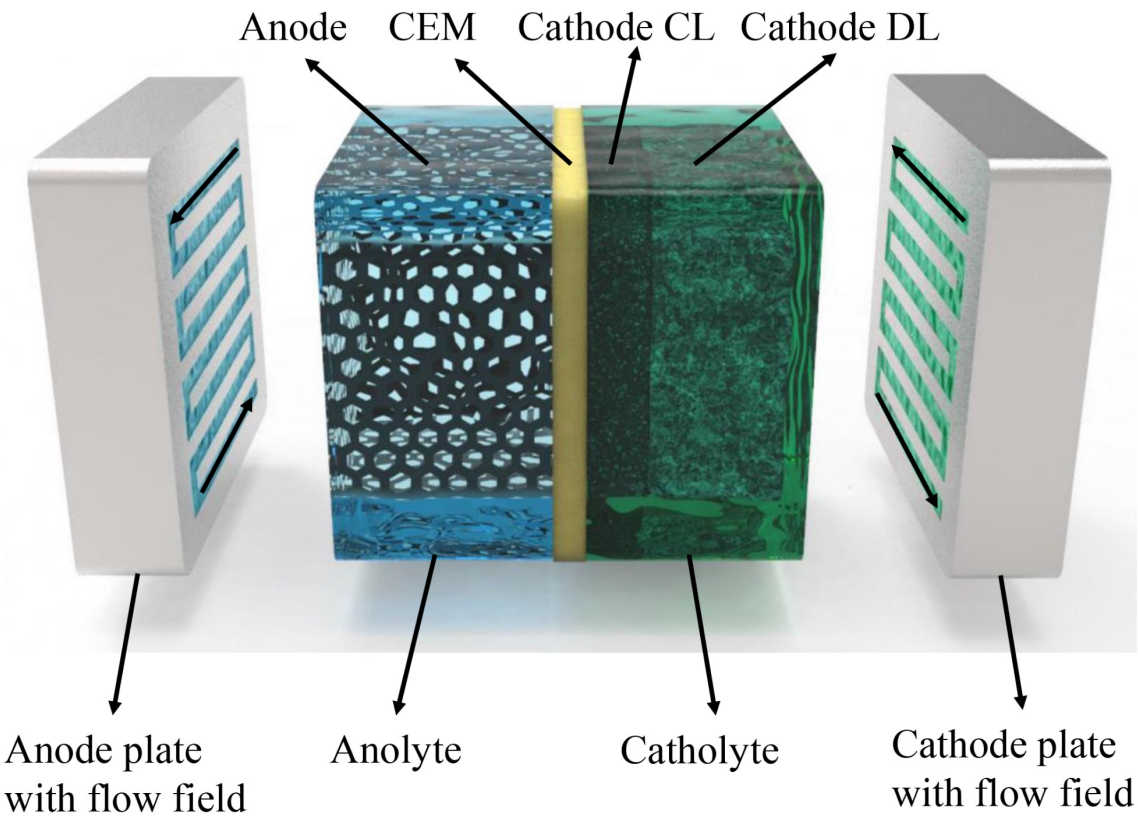

Fig. 1 Working principle of an active alkaline-acid direct ethylene glycol fuel cell.

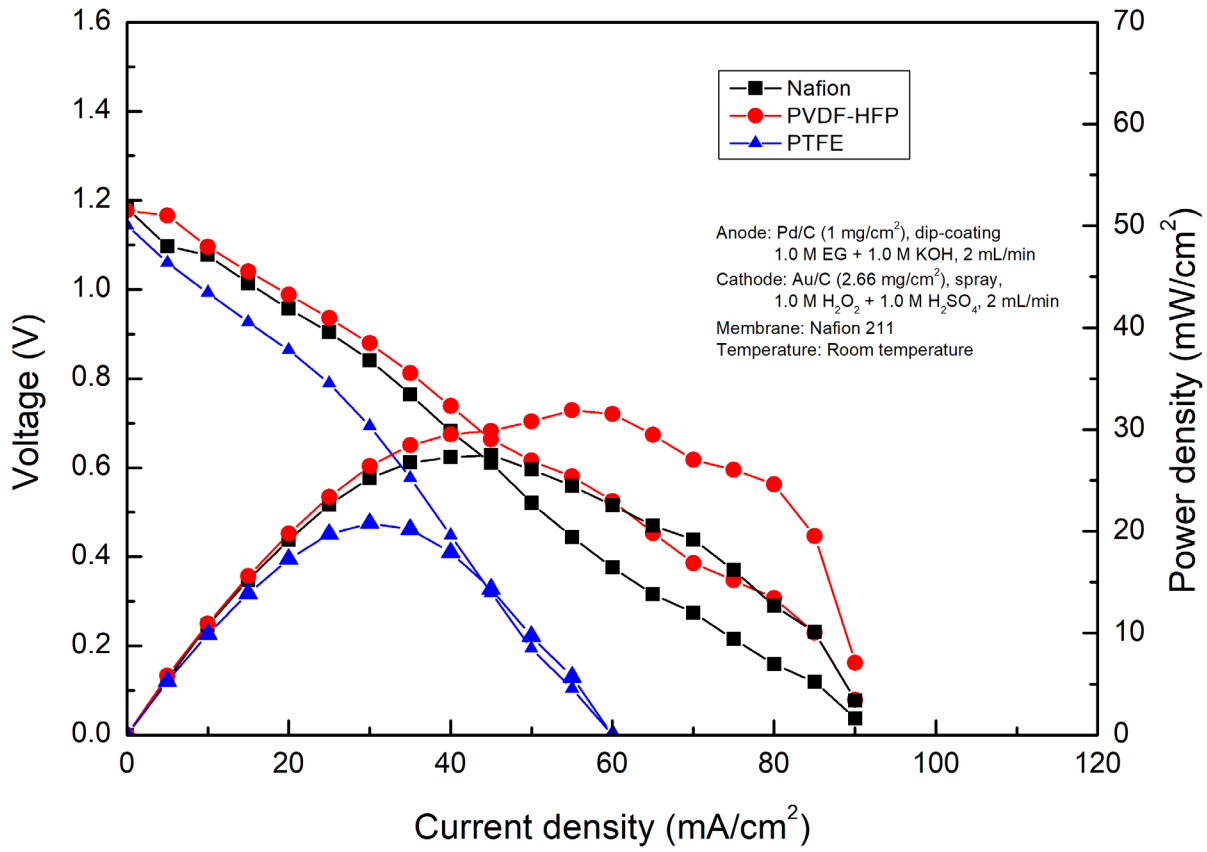

Fig. 2 Fuel cell performances achieved by using different binders at room temperature.

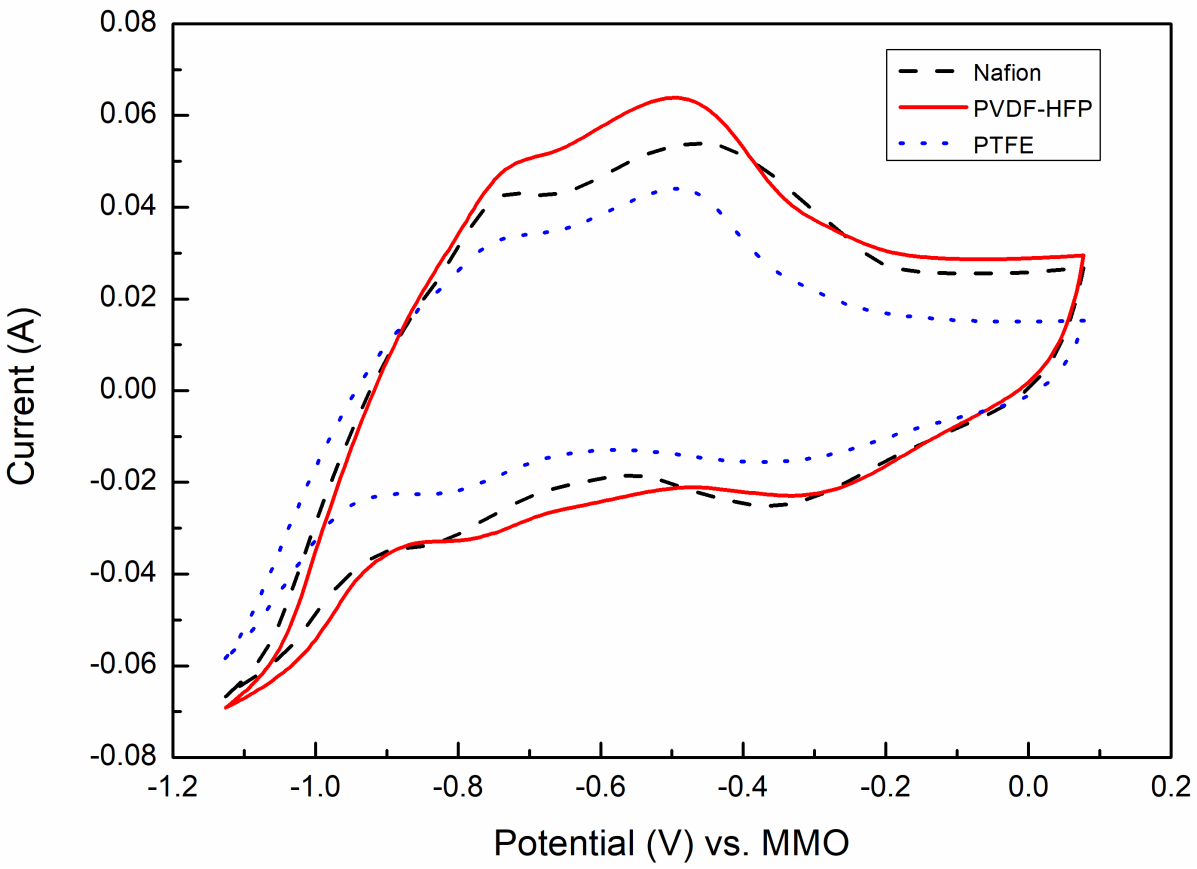

Fig. 3 CV curves in 1.0 M KOH at a scan rate of 50 mV s^{-1}.

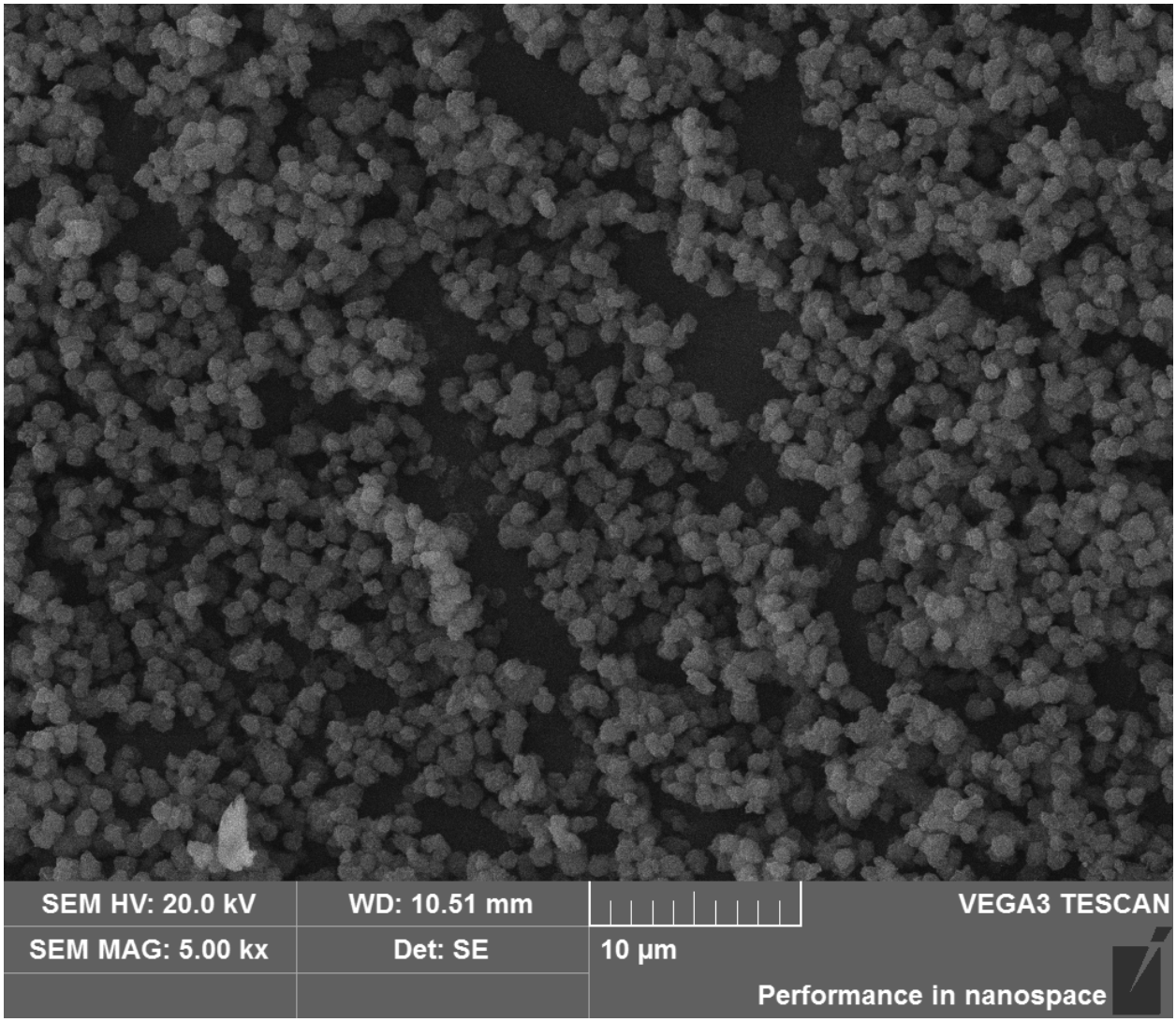

Fig. 4 (a) SEM image of the PVDF-HFP at dry state.

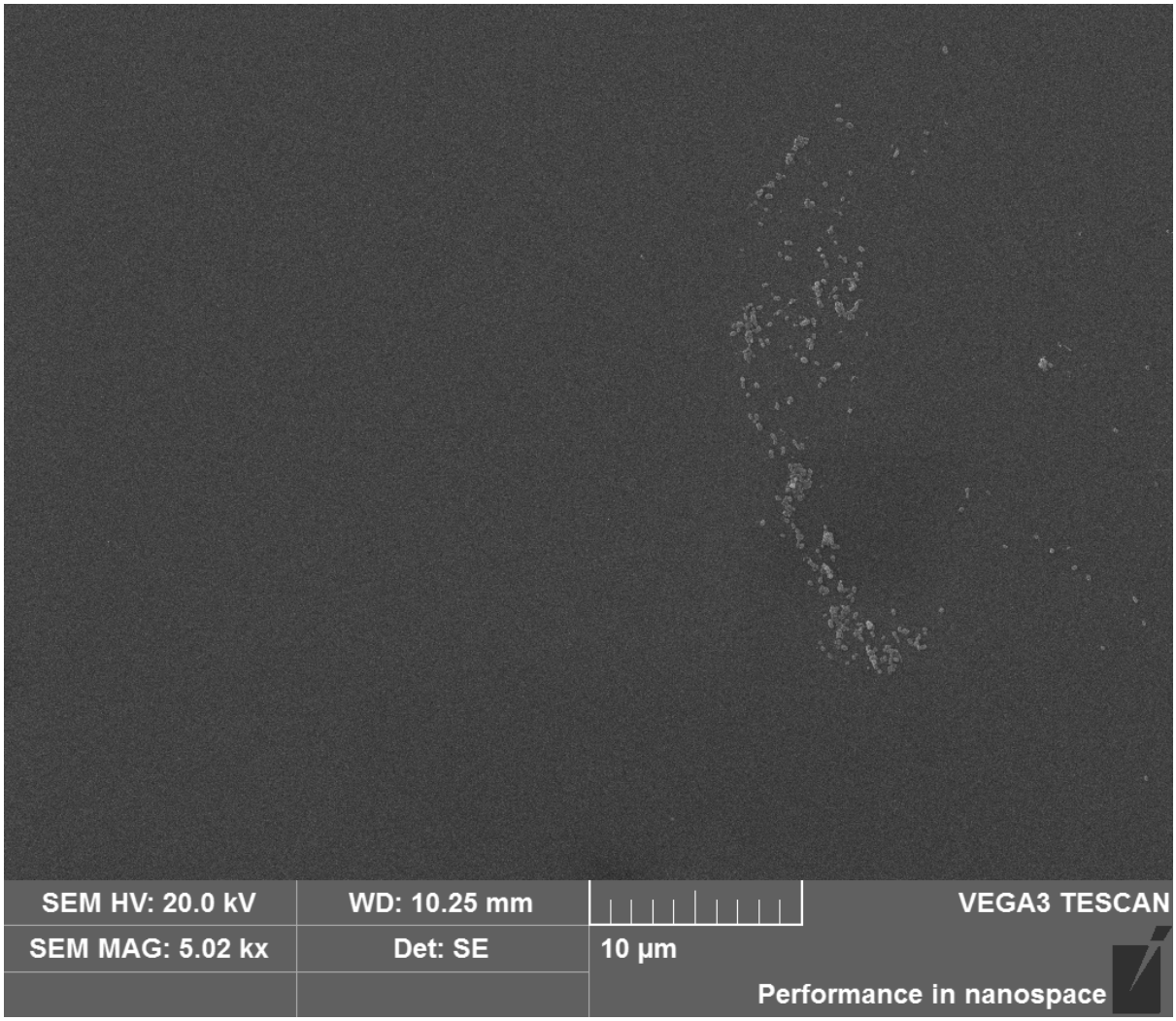

Fig. 4 (b) SEM image of the Nafion at dry state.

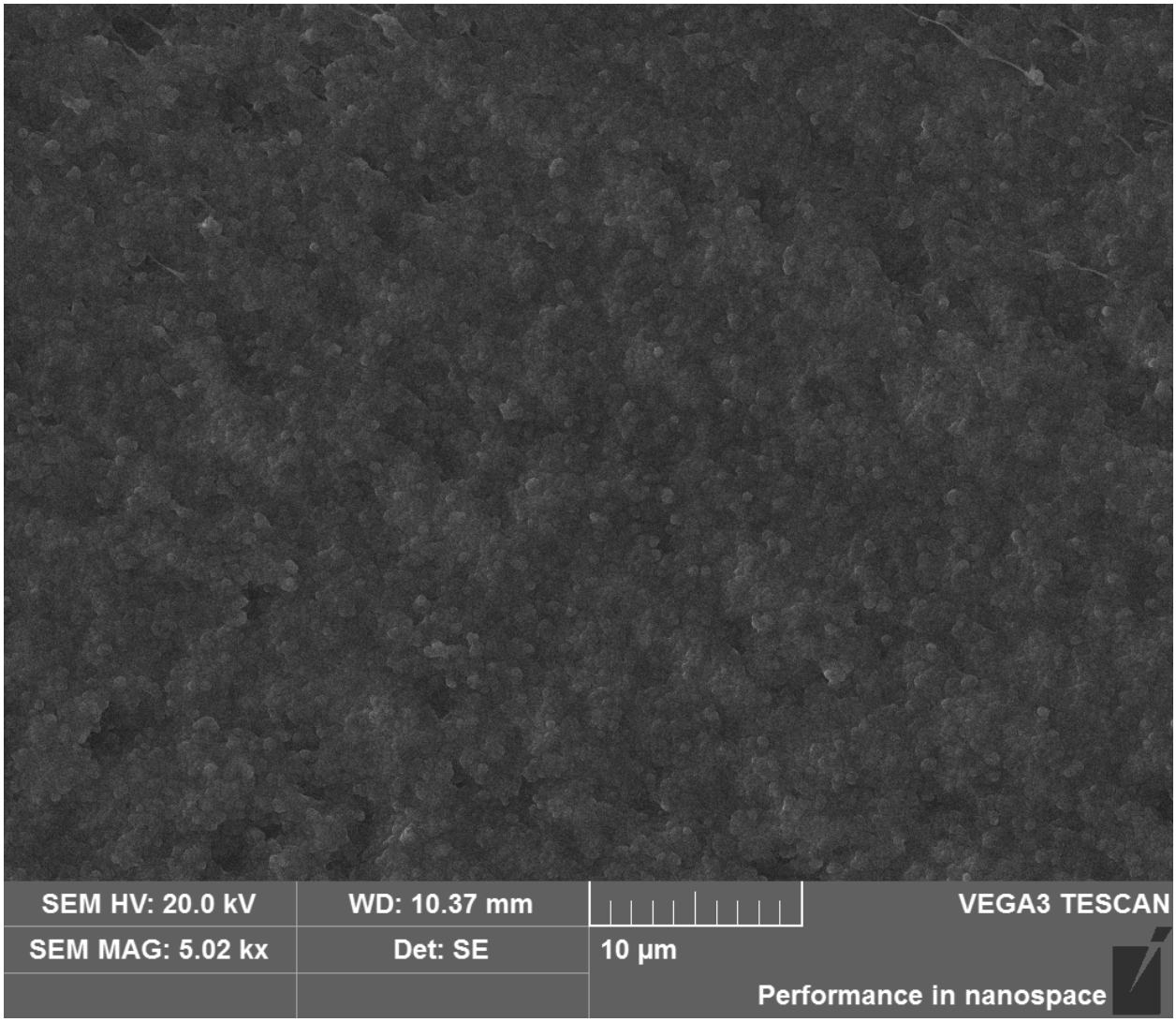

Fig. 4 (c) SEM image of the PTFE at dry state.

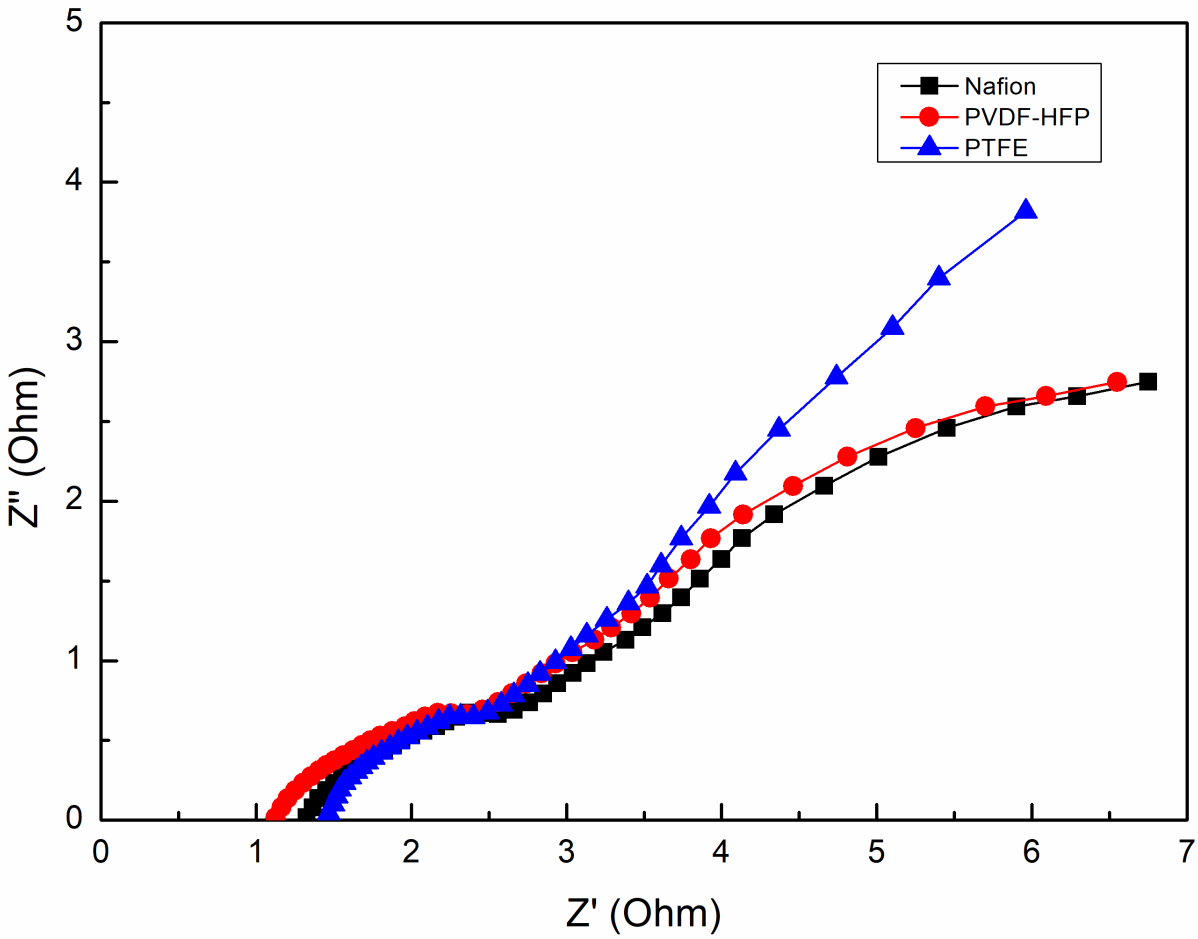

Fig. 5 Nyquist plots of three different electrodes at room temperature.

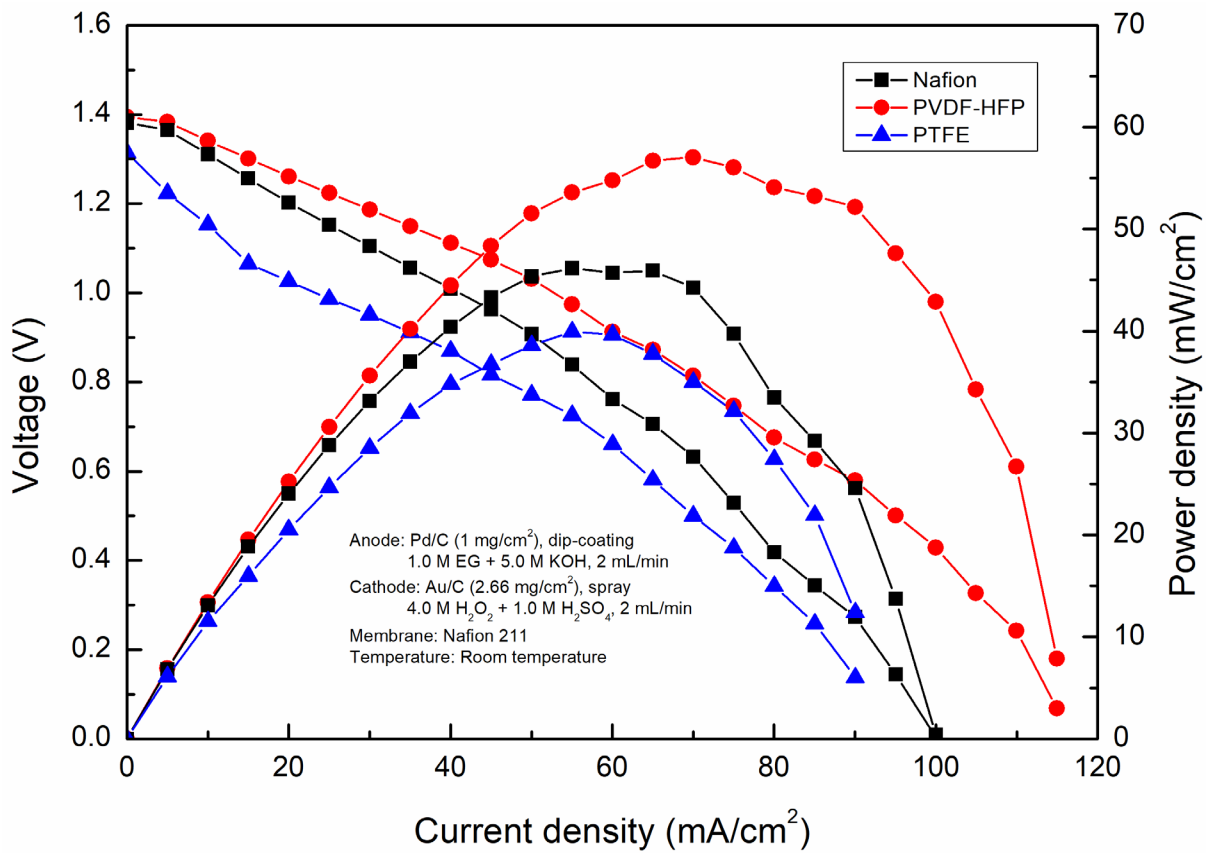

Fig. 6 Polarization and power density curves achieved by using three different electrodes at room temperature.

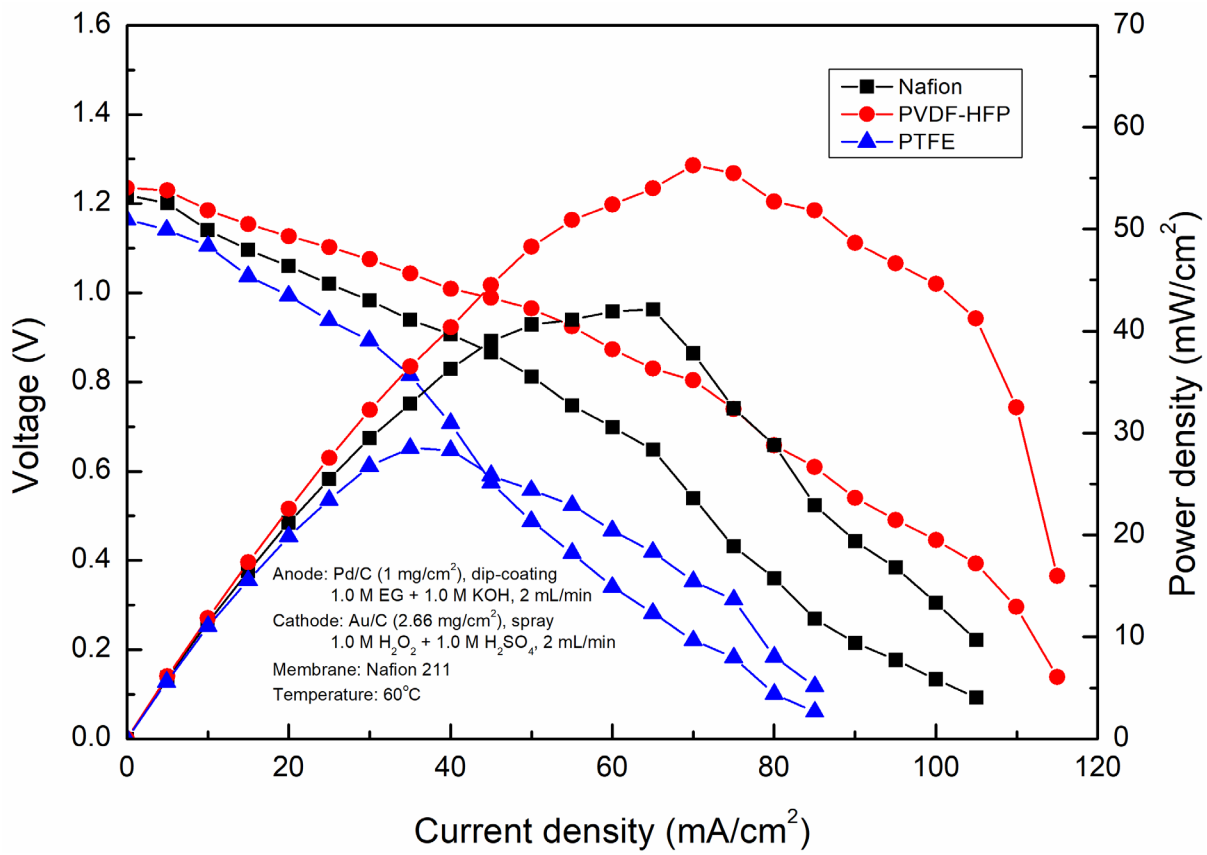

Fig. 7 Polarization and power density curves achieved by using three different electrodes at 60°C.

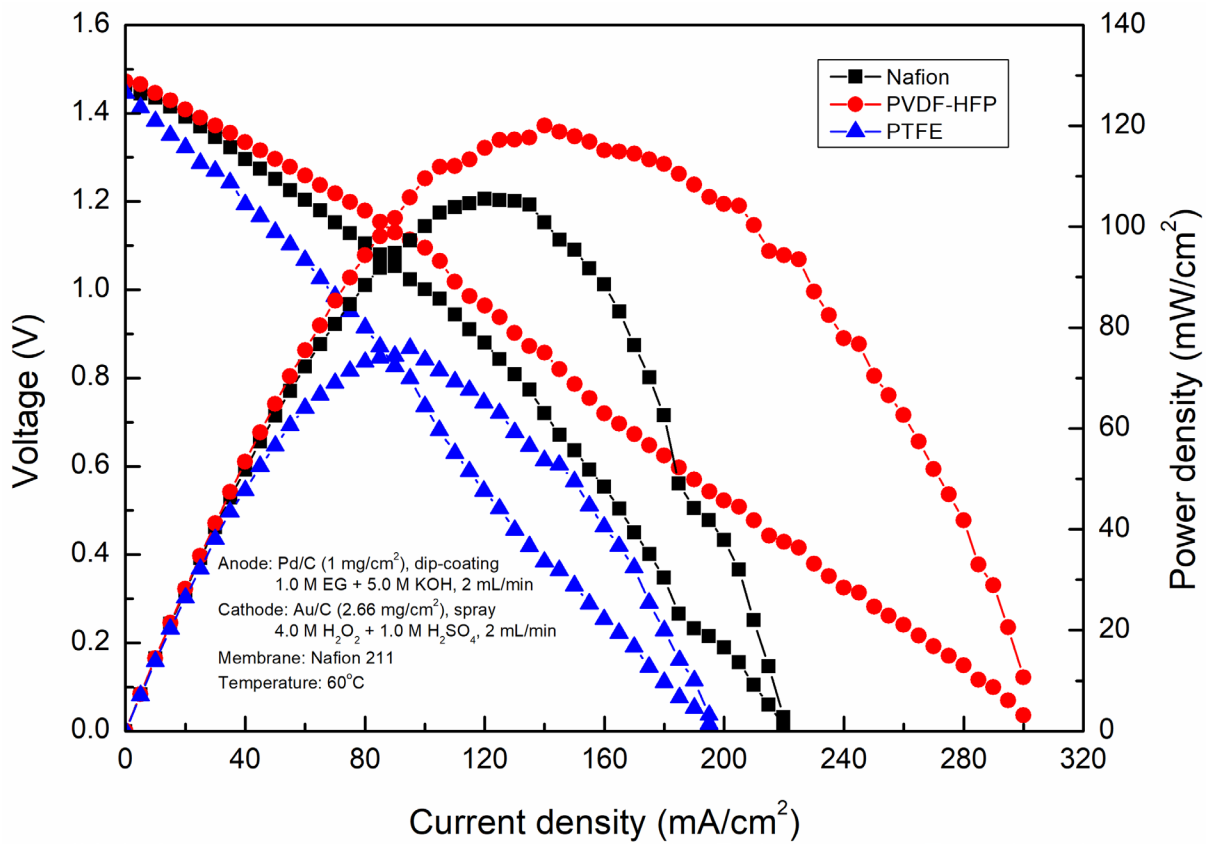

Fig. 8 Polarization and power density curves achieved by using three different electrodes at 60°C.

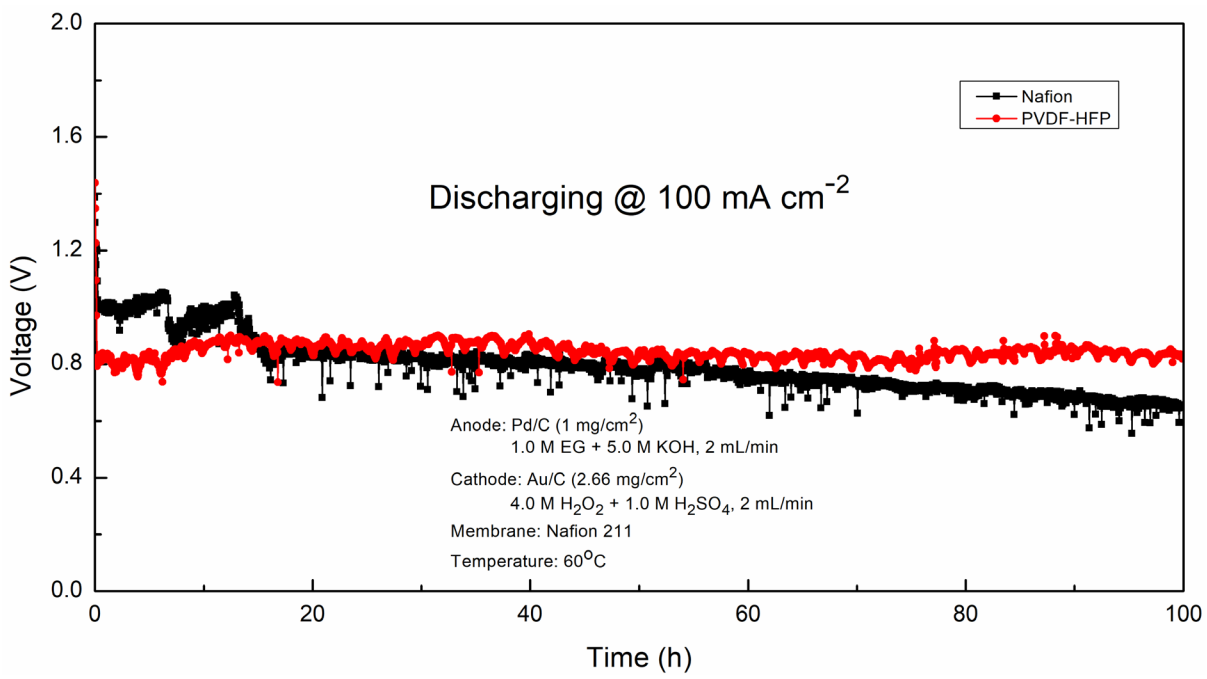

Fig. 9 Transient discharging behavior of the fuel cell fabricated with the PVDF-HFP-based and Nafion-based electrodes at 60^{o}C.